CHINESE OPTICS LETTERS

Vol. 21, No. 4 | April 2023

Real-time suppression of random phase drift for laser ranging with high-frequency intermode beats

Ruitao Yang (杨睿韬)[1,2,†], Hao Sun (孙 昊)[1,2,†], Pengcheng Hu (胡鹏程)[1,2*], Hongxing Yang (杨宏兴)[1,2], Haijin Fu (付海金)[1,2], Liang Yu (于 亮)[1,2], Xu Xing (邢 旭)[1,2], Xuemei Ding (丁雪梅)[1,2], and Jiubin Tan (谭久彬)[1,2]

[1] Center of Ultra-precision Optoelectronic Instrument, Harbin Institute of Technology, Harbin 150080, China

[2] Key Laboratory of Ultra-precision Intelligent Instrumentation (Harbin Institute of Technology), Ministry of Industry and Information Technology, Harbin 150080, China

*Corresponding author: hupc@hit.edu.cn

Received October 11, 2022 | Accepted November 28, 2022 | Posted Online April 3, 2023

Laser ranging with frequency comb intermode beats (IMBs) has been suffering from random phase drifts (RPDs) for two decades. In this study, we reveal the influence of signal transmission path on the RPDs and propose a real-time suppression method using two IMBs of similar frequencies from different combs. As the two IMBs obtain similar RPDs during their transmission through same signal paths, the RPD of the original probing signal IMB is suppressed by deducting the RPD of the newly added local IMB in real time. In our experiments, a real-time suppression of RPDs is achieved using IMBs of 1001 and 1000 MHz. For the sampling time of 100 s, the effect of 19-fold suppression has been achieved. The proposed method provides a new solution for the long-standing phase drift problem in laser ranging with comb IMBs.

Keywords: intermode beat; random phase drift; laser ranging.

DOI: 10.3788/COL202321.041202

1. Introduction

Optical frequency combs provide bidirectional time traceability chains between the optical and electrical domains[1]. The time base from microwaves to optical waves is transmitted via the comb phase locking of both repetition rate (REP) and carrier-envelope phase (CEP)[2,3]. In reverse, the optical time base is transmitted back to the electrical domain via various comb-based measurement methods[4–6]. As the first absolute distance measurement method based on optical frequency comb, ranging with comb intermode beats (IMBs) has the unique advantages in terms of direct traceability and a simple principle[7–11]. With the phases of IMBs, the distance information is related to the REP and its higher-order harmonics of the frequency comb only. Since the REP can be detected and stabilized referencing to the time standard directly, ranging with the comb IMBs has attracted wide attention, particularly in space missions[8].

For this ranging method, high resolution requires a high-frequency IMB. However, the phase measurement of high-frequency IMBs is subject to the random phase drift (RPD) induced in signal transmission. The RPD is accumulated and aggravated in long-term continuous ranging. The RPD can be monitored by alternately detecting the measurement signal and a phase-constant compensating signal[9,10]. Thus, the RPD can be compensated at the cost of the measurement speed. Another solution uses frequency-modulated IMBs[11] to filter the drift by decomposing and reconstructing the phase signal via offline processing of measurement data. Its principle hinders the applications of real-time measurement.

In this Letter, we suppress the RPD of the comb IMBs in real time using two IMBs with similar frequencies from different combs. In Section 2, we theoretically analyze RPD sources in conventional methods and then propose a real-time suppression method. The proposed method requires one signal comb to probe the target and another local comb to monitor the RPD in real time. The phase difference measurement of the two IMBs is equivalent to the phase measurement of the probing signal comb IMBs, yet with the RPD deeply suppressed. In Section 3, a real-time suppression experiment is demonstrated using the two IMBs at 1001 and 1000 MHz. To characterize the RPD and isolate the phase jitter effect, data are analyzed with Allan deviation at a relatively longer sampling time. After the suppression, the RPD is merely 1 μm at a 100 s sampling time, with a 19-fold suppression realized.

2. Analysis and Method

To analyze the RPD sources, Fig. 1 shows a typical example of the signal processing in ranging with the comb IMBs. The frequency comb is separated into the measurement and reference paths, respectively. The IMBs from both paths are detected to

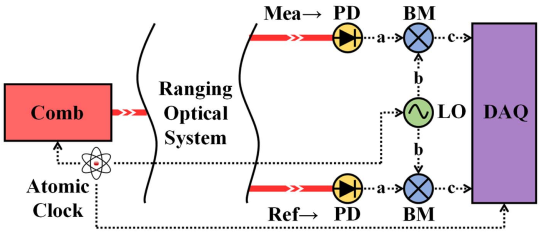

Fig. 1. Typical example of downconversion signal processing in ranging with comb IMBs. Mea, measurement signal; Ref, reference signal; PD, photodetector; BM, balanced mixer; LO, local oscillator; DAQ, data acquisition.

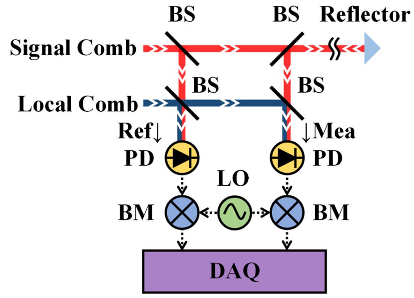

Fig. 2. System diagram of the real-time RPD suppression. BS, beam splitter.

extract the distance-related relative phase shift φ_0[7]. Limited to the maximum sample rate of the data acquisition (DAQ) module for only hundreds of megahertz, the IMB with its frequency f_{IMB} over gigahertz needs downconversion signal processing. By mixing with the local oscillator (LO) signal (f_{LO}, slightly lower than f_{IMB}) at the balanced mixers (BMs), the beats of f_{IMB} are downconverted into the intermediate frequency (IF) signals of $f_{\mathrm{IMB}} - f_{\mathrm{LO}}$. The atomic clock transmits the time base to the comb, LO, and DAQ modules.

To reveal the source of RPD, the signal transmission path of IMBs should be analyzed. In the measurement of phase shift φ_0, extra phase shifts are introduced from the signal transmission of path–a (PDs to BMs), path–b (LO to BMs), and path–c (BMs to DAQ). One part of the extra phase shifts is induced by the intrinsic time delays of the three paths (a, b, and c) including the electrical components, cables, and interfaces. The other part is induced by random time delays due to environmental factors. The phase shift φ of the eventual IF signals, instead of the initial φ_0, determines the IMB phase measurement results,

$$\varphi = \varphi_0 + \varphi_{\mathrm{ITD}} + \delta\varphi_{\mathrm{RTD}}, \tag{1}$$

where φ_{ITD} and $\delta\varphi_{\mathrm{RTD}}$ denote the phase shifts induced by the intrinsic and random time delays, respectively. The expression of φ_{ITD} is

$$\varphi_{\mathrm{ITD}} = 2\pi[f_{\mathrm{IMB}} t_{\mathrm{a}} + f_{\mathrm{LO}} t_{\mathrm{b}} + (f_{\mathrm{IMB}} - f_{\mathrm{LO}}) t_{\mathrm{c}}], \tag{2}$$

where t_{a}, t_{b}, and t_{c} denote the relative intrinsic time delays between the measurement and reference signals induced from path–a, path–b, and path–c, respectively. The intrinsic phase shift φ_{ITD} can be eliminated by zero calibration. Likewise, the relative random time delays between the measurement and reference signals are, respectively, denoted as δt_{a}, δt_{b}, and δt_{c}. According to Eq. (2), $\delta\varphi_{\mathrm{RTD}}$ can be expressed as

$$\delta\varphi_{\mathrm{RTD}} = 2\pi[f_{\mathrm{IMB}} \delta t_{\mathrm{a}} + f_{\mathrm{LO}} \delta t_{\mathrm{b}} + (f_{\mathrm{IMB}} - f_{\mathrm{LO}}) \delta t_{\mathrm{c}}]. \tag{3}$$

Equation (3) explains the sources of the RPD $\delta\varphi_{\mathrm{RTD}}$ induced in the ranging with comb IMBs. As the random time delays change in real time, existing methods make it difficult to eliminate such error sources thoroughly.

Based on the aforementioned error source analysis, a system diagram of the real-time RPD suppression is proposed in Fig. 2. The signal comb generates the IMB with the frequency of f_{IMB} at the PDs and carries the distance-dependent phase shift φ_0 in the beats of f_{IMB}. The local comb generates a similar frequency f_{IMBL} and carries a constant phase shift $\varphi_{0\mathrm{L}}$ in the beats of f_{IMBL} due to the fixed-distance propagation, assuming $f_{\mathrm{IMB}} > f_{\mathrm{IMBL}} > f_{\mathrm{LO}}$. The beats f_{IMBL} are downconverted in sync with the beats of f_{IMB}. According to Eq. (1), the phase shift φ_{L} of the IF signals ($f_{\mathrm{IMBL}} - f_{\mathrm{LO}}$) of the beats f_{IMBL} can be expressed as

$$\varphi_{\mathrm{L}} = \varphi_{0\mathrm{L}} + \varphi_{\mathrm{ITDL}} + \delta\varphi_{\mathrm{RTDL}}, \tag{4}$$

where φ_{ITDL} denotes the phase shift induced by the intrinsic time delays for the beats of f_{IMBL}. The phase drift $\delta\varphi_{\mathrm{RTDL}}$ induced by the random time delays δt_{aL}, δt_{b}, and δt_{cL} from path–a, –b, and –c can be expressed as

$$\delta\varphi_{\mathrm{RTDL}} = 2\pi[f_{\mathrm{IMBL}} \delta t_{\mathrm{aL}} + f_{\mathrm{LO}} \delta t_{\mathrm{b}} + (f_{\mathrm{IMBL}} - f_{\mathrm{LO}}) \delta t_{\mathrm{cL}}]. \tag{5}$$

The random time delays δt_{aL}, δt_{b}, and δt_{cL} are related to the signal frequencies[12,13]. Considering $\delta t_{\mathrm{aL}} \approx \delta t_{\mathrm{a}}$ and $\delta t_{\mathrm{cL}} \approx \delta t_{\mathrm{c}}$ due to the similar frequencies of f_{IMB} and f_{IMBL}, the phase drift $\delta\varphi_{\mathrm{RTDL}}$ can be approximated as

$$\delta\varphi_{\mathrm{RTDL}} \approx 2\pi[f_{\mathrm{IMBL}} \delta t_{\mathrm{a}} + f_{\mathrm{LO}} \delta t_{\mathrm{b}} + (f_{\mathrm{IMBL}} - f_{\mathrm{LO}}) \delta t_{\mathrm{c}}]. \tag{6}$$

When the phase φ_{L} is subtracted from the phase φ, the result is

$$\varphi - \varphi_{\mathrm{L}} = \varphi_0 + (-\varphi_{0\mathrm{L}} + \varphi_{\mathrm{ITD}} - \varphi_{\mathrm{ITDL}}) + (\delta\varphi_{\mathrm{RTD}} - \delta\varphi_{\mathrm{RTDL}}). \tag{7}$$

There is a total of three items in Eq. (7). The first item is the phase φ_0 to be measured. The second item $-\varphi_{0\mathrm{L}} + \varphi_{\mathrm{ITD}} - \varphi_{\mathrm{ITDL}}$ is the equivalent intrinsic phase shift, which can be eliminated by zero calibration. And the third item can be further simplified according to Eqs. (3) and (6) as

$$\delta\varphi_{\mathrm{RTD}} - \delta\varphi_{\mathrm{RTDL}} \approx 2\pi(f_{\mathrm{IMB}} - f_{\mathrm{IMBL}})(\delta t_{\mathrm{a}} + \delta t_{\mathrm{c}}). \tag{8}$$

Compared with Eq. (3), the RPD $\delta\varphi_{\mathrm{RTD}} - \delta\varphi_{\mathrm{RTDL}}$ in Eq. (8) has fewer error sources (with the common mode $f_{\mathrm{LO}} \times \delta t_{\mathrm{b}}$ canceled) and is easier to suppress by reducing $f_{\mathrm{IMB}} - f_{\mathrm{IMBL}}$. In summary, the second and third items of Eq. (7) can be calibrated and minimized, respectively. Therefore, the measurement of the phase shift difference of the IMB of f_{IMB} and f_{IMBL} in Eq. (7) is equivalent to the measurement of φ_0. As both phases φ and φ_{L} can be obtained from the measurement, the RPD can be suppressed in real time.

3. Experiments

Figure 3 demonstrates the experimental setup of ranging with the comb IMBs suppressing the RPD in real time. The signal comb is based on a self-made mode-locked laser with an REP of 43.52 MHz, whereas the local comb is a commercial one with a 250 MHz REP. Four polarization beam splitters (PBSs) determine the beam direction, as indicated by white arrows. With the signal comb beam (colored in red) split by PBS–1, the reflected light (namely, the reference beam) is received by the reference PD, whereas the transmitted light (namely, the measurement beam) probes the target reflector and then returns to the measurement PD. Thus, the signal comb carries distance-dependent phase information in the IMBs. Meanwhile, the local comb carries a constant phase in the beats, with the beams (colored in blue) propagating at a fixed distance. The extraction of phase information requires that the IMBs generated by the PDs be downconverted. The 23rd-order beats of the signal comb (with a frequency of $f_{\mathrm{IMB}} = 1001$ MHz) and the fourth-order beats of the local comb ($f_{\mathrm{IMBL}} = 1000$ MHz) are downconverted by mixing with the LO signal ($f_{\mathrm{LO}} = 1000.48$ MHz) at the BMs. The LO signal is distributed to both BMs with the same output channel of the signal generator and a power splitter (PS) to ensure the processing synchronization of the measurement and reference signals. The atomic time base is transmitted to the combs (with the REP phase-locked rather than the CEP), LO, and DAQ modules for synchronization.

It should be noted that the accurate phase measurement of IMBs requires the PDs to operate in the linear region[14]. Otherwise, saturated PDs will introduce dynamic phase retardation related to the pulse energy fluctuation[15] into the initial phase shift φ_0 and $\varphi_{0\mathrm{L}}$. At the same time, the signal comb with relatively low REP is easier to saturate the PDs and BMs, introducing extra phase errors[16]. Thus, there are six half-wave plates and a quarter-wave plate in our experimental setup to optimize the incident optical power of the PDs. Meanwhile, the signals output from the PDs are filtered by 1 GHz bandpass filters to prevent the saturation of BMs. In addition, the attitudes of PBS–1 and PBS–2 are intentionally slightly tilted. Thus, the polarization leakage of the reference beam of the signal comb reflected from PBS–2 is deviated away from PBS–4 and cannot be detected by the measurement PD, avoiding cyclical error[17].

To identify the linear operation region, the radio-frequency (RF) response of the PDs is studied. Figure 4 depicts the response of the measurement PDs detecting the two combs separately or simultaneously. Both PDs are the identical model (Menlo Systems APD310, with a bandwidth of 1.6 GHz) and hence have nearly the same response curves. The linear region (shadowed in green) and the nonlinear region (shadowed in yellow) can be distinguished from each curve in Fig. 4. Taking Fig. 4(a) as an example, the signal comb (43.52 MHz REP) is detected individually by the measurement PD. In the linear region, the RF power of the IMB of f_{IMB} is highly proportional to the square of the incident optical power. In the nonlinear region, the PD is saturated, with the curve reaching a plateau and then varying irregularly[14]. Figure 4(b) records the RF power of the beat of f_{IMBL} when the local comb (250 MHz REP) is detected individually. Comparing the linear regions of Figs. 4(a) and 4(b), the local comb provides much higher RF power ($P_{1\ \mathrm{dB}} = -26$ dBm) than the signal comb ($P_{1\ \mathrm{dB}} = -35$ dBm) for the beats with similar frequencies ($f_{\mathrm{IMB}}=$ 1001 MHz and $f_{\mathrm{IMBL}} = 1000$ MHz). This RF power difference is attributed to the REP difference in the two combs[18]. The maximum RF power in the linear region further decreases when detecting the combs simultaneously [with the optical power ratio of 1:1; Figs. 4(c) and 4(d)]. Besides the saturation of PDs and BMs, the power of both IF signals should be carefully

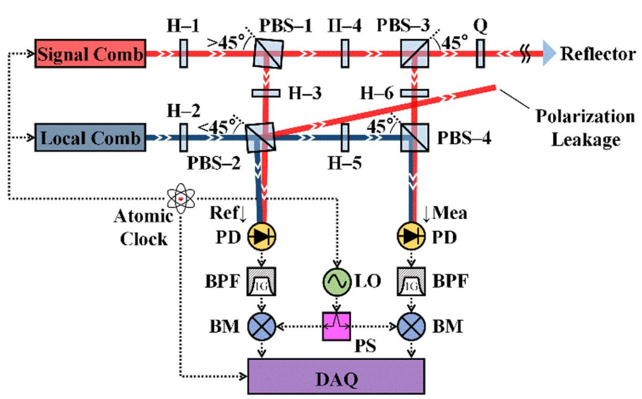

Fig. 3. Experimental setup of ranging with the comb IMBs suppressing the RPD in real time. PBS, polarization beam splitter; H, half-wave plate; Q, quarter-wave plate; PS, power splitter; BPF, bandpass filter.

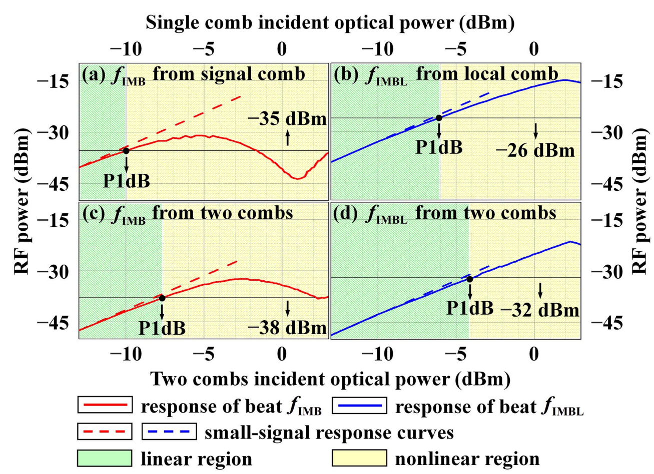

Fig. 4. RF response of the measurement PD. (a) Beat f_{IMB} with the signal comb detected individually; (b) beat f_{IMBL} with the local comb detected individually; (c) beat f_{IMB} and (d) beat f_{IMBL} with the two combs (of the same optical power) detected simultaneously. $P_{1\ \mathrm{dB}}$, RF power at the 1-dB compression point.

optimized to minimize their interaction in the phase measurement. To achieve this target in our experiment, the optical power and power ratio of the two combs are carefully adjusted with the wave plates. Eventually, the RF power of each beat (f_{IMB} and f_{IMBL}) from each PD is equalized to approximately −43 dBm. The amplitude of each resulting IF signal ($f_{IMB} - f_{LO}$ or $f_{IMBL} - f_{LO}$) is 1 mV (with a power of −55 dBm). Here, the low power of the IF signal and the noise floor of the DAQ will be the main factors affecting the ranging precision, rather than the phase noise of the IF signal itself. With the help of higher REP combs, the IF power can be further increased in the future.

Figure 5 shows the experimental results of the real-time RPD suppression. The reflector target is fixed at a short distance of about 0.5 m to reduce the influence on the RPD from the air refractive index variation and the foundation thermal expansion. The distance variation is continuously measured with the IMBs for 40 min and updated every 0.5 s with the acquiring time of 20 ms. Figure 5(a) compares the results without (colored in red) and with (colored in black) the real-time suppression. During the measurement, artificial disturbances were imposed to simulate a severe environment. A section of signal-transmission cable was gripped in hand for warming up rapidly and bending to simulate violent temperature changes and thermal deformation. In this process, the measurement result drifted for up to 150 μm. Meanwhile, the effect of vibration was simulated by knocking on the cables at the 25th minute, and an instant rise of about 50 μm was observed in the curve. For the other times, the measurement result drifted relatively slowly, mainly attributed to slight room temperature fluctuations. Comparatively, the measurement results with the suppression were much stabler. The effects of gripping and knocking could not be identified from the suppressed results, indicating the proposed method works effectively on the drifts and instant changes. Figure 5(b) gives the Y-scale zoom-in details of the suppressed results in Fig. 5(a). The overall distance variation is about 55 μm. However, the method is proposed to suppress the relatively long-term RPD. Therefore, the suppressed results are smoothed by a 10 s adjacent-averaging. Accordingly, the peak-to-peak fluctuation of the corresponding green curve in Fig. 5(b) is down to 20 μm, significantly decreasing from the total drift of 220 μm for the red curve in Fig. 5(a). To show the long-term drift suppression effect quantitatively and mitigate the influence of the short-term jitters, the measurement results are analyzed with Allan deviation, as shown in Fig. 5(c)[19]. With the increasing of sampling time from 0.5 s to 100 s, the Allan deviation of the original result first decreases from 6 μm (0.5 s) to 3 μm (5 s) and then increases up to 19 μm (100 s). When the proposed method is applied, the same condition Allan deviation of the suppressed result decreases from 8 μm (0.5 s) to 1 μm (100 s) monotonically. The 100 s long-term Allan deviation has been reduced to 1/19 of the original data, further proving the effectiveness of the drift suppression.

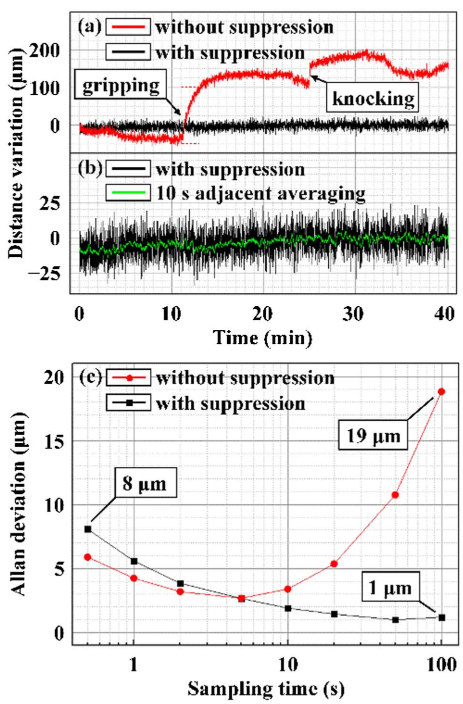

Fig. 5. Experimental results of real-time RPD suppression. (a) Comparison of the distance variation measurement results without and with the real-time suppression; (b) zoom-in details of the suppressed results in the Y-scale; (c) Allan deviation of the measurement results with and without the RPD suppression.

4. Conclusion

We propose a real-time suppression method for the RPD in ranging with high-frequency comb IMBs. The mechanism of RPD generation is analyzed and modeled from the aspect of signal transmission. Two IMBs of similar frequencies from different combs are applied to suppress the RPD. The drift suppression performance is quantitatively evaluated using Allan deviation. For the 100 s sampling time, the Allan deviation is suppressed from 19 to 1 μm with the proposed method. The proposed method provides a new solution for the long-standing phase drift problem in laser ranging with high-frequency comb IMBs. Although the PDs are easier to be saturated by the two combs, we believe combs with higher REPs will solve the problem and further improve measurement precision. For the future, we are looking forward to realizing high-REP combs with ultrashort fiber cavities.

Acknowledgement

This work was supported by the National Natural Science Foundation of China (NSFC) (Nos. 52175501 and 51605120), the Heilongjiang Provincial Natural Science Foundation (No. LH2021E059), and the National Key Research and Development Program of China (No. 2020YFC2200204).

†These authors contributed equally to this work.

References

1. J. Ye, H. Schnatz, and L. W. Hollberg, "Optical frequency combs: from frequency metrology to optical phase control," IEEE J. Sel. Top. Quantum Electron. **9**, 1041 (2003).
2. J. Kim and Y. Song, "Ultralow-noise mode-locked fiber lasers and frequency combs: principles, status, and applications," Adv. Opt. Photonics **8**, 465 (2016).
3. F. W. Helbing, G. Steinmeyer, and U. Keller, "Carrier-envelope offset phase-locking with attosecond timing jitter," IEEE J. Sel. Top. Quantum Electron. **9**, 1030 (2003).
4. R. Yang, F. Pollinger, K. Meiners-Hagen, J. Tan, and H. Bosse, "Heterodyne multi-wavelength absolute interferometry based on a cavity-enhanced electro-optic frequency comb pair," Opt. Lett. **39**, 5834 (2014).
5. Z. Zhu and G. Wu, "Dual-comb ranging," Engineering **4**, 772 (2018).
6. T. Fortier and E. Baumann, "20 years of developments in optical frequency comb technology and applications," Commun. Phys. **2**, 153 (2019).
7. K. Minoshima and H. Matsumoto, "High-accuracy measurement of 240-m distance in an optical tunnel by use of a compact femtosecond laser," Appl. Opt. **39**, 5512 (2000).
8. Y.-S. Jang, W. Kim, H. Jang, and S.-W. Kim, "Absolute distance meter operating on a free-running mode-locked laser for space mission," Int. J. Precis. Eng. Manuf. **19**, 975 (2018).
9. D. Salido-Monzú and A. Wieser, "Simultaneous distance measurement at multiple wavelengths using the intermode beats from a femtosecond laser coherent supercontinuum," Opt. Eng. **57**, 044107 (2018).
10. N. R. Doloca, K. Meiners-Hagen, M. Wedde, F. Pollinger, and A. Abou-Zeid, "Absolute distance measurement system using a femtosecond laser as a modulator," Meas. Sci. Technol. **21**, 115302 (2010).
11. X. Xu, Z. Zhang, H. Zhang, H. Zhao, W. Xia, M. He, J. Li, J. Zhai, and H. Wu, "Long distance measurement by dynamic optical frequency comb," Opt. Express **28**, 4398 (2020).
12. R. Papazyan and R. Eriksson, "Calibration for time domain propagation constant measurements on power cables," IEEE Trans. Instrum. Meas. **52**, 415 (2003).
13. S. Yokoyama, A. Okamoto, T. Araki, and N. Suzuki, "Examination to eliminate undesirable phase delay of an avalanche photodiode (APD) for intensity-modulated light," Rev. Sci. Instrum. **66**, 5331 (1995).
14. R. Bouchand, D. Nicolodi, X. Xie, C. Alexandre, and Y. L. Coq, "Accurate control of optoelectronic amplitude to phase noise conversion in photodetection of ultra-fast optical pulses," Opt. Express **25**, 12268 (2017).
15. M. Currie and I. Vurgaftman, "Microwave phase retardation in saturated InGaAs photodetectors," IEEE Photon. Technol. Lett. **18**, 1433 (2006).
16. T. Bosch and M. Lescure, "Crosstalk analysis of 1 m to 10 m laser phase-shift range finder," IEEE Trans. Instrum. Meas. **46**, 1224 (1997).
17. H. Fu, Y. Wang, P. Hu, J. Tan, and Z. Fan, "Nonlinear errors resulting from ghost reflection and its coupling with optical mixing in heterodyne laser interferometers," Sensors **18**, 758 (2018).
18. H. Jiang, J. Taylor, F. Quinlan, T. Fortier, and S. A. Diddams, "Noise floor reduction of an Er:fiber laser-based photonic microwave generator," IEEE Photonics J. **3**, 1004 (2011).
19. D. Allan, "Statistics of atomic frequency standards," Proc. IEEE **54**, 221 (1966).